

High-power waveguide resonator second harmonic device with external conversion efficiency up to 75%

M Stefszky¹ , R Ricken, C Eigner, V Quiring, H Herrmann and C Silberhorn 

Integrated Quantum Optics, Applied Physics, University of Paderborn, Warburger Strasse 100, D-33098 Paderborn, Germany

E-mail: stefszky@mail.upb.de

Received 8 December 2017, revised 11 April 2018

Accepted for publication 2 May 2018

Published 14 May 2018



CrossMark

Abstract

We report on a highly efficient waveguide resonator device for the production of 775 nm light using a titanium indiffused LiNbO₃ waveguide resonator. When scanning the resonance, the device produces up to 110 mW of second harmonic power with 140 mW *incident* on the device—an external conversion efficiency of 75%. The cavity length is also locked, using a Pound–Drever–Hall type locking scheme, involving feedback to either the cavity temperature or the laser frequency. With laser frequency feedback, a stable output power of approximately 28 mW from a 52 mW pump is seen over one hour.

Keywords: nonlinear optics, integrated optics, optical waveguides, second harmonic generation

(Some figures may appear in colour only in the online journal)

1. Introduction

Integrated optical waveguide technologies offer improvements in size, scalability, integrability and nonlinear efficiency over their bulk counterparts. These properties have been used to create a myriad of impressive devices, such as high-speed switches [1], optical parametric oscillators [2], sources of optical squeezing [3, 4] and frequency conversion devices [5]. Frequency conversion is often used to produce laser fields at wavelengths inaccessible to current materials [6], but can also be used to interface individual parts of a network [5] or to transfer information from one field to another at a different wavelength [7].

Traditionally, the main advantage of waveguide devices has been very high nonlinear efficiency, allowing for relatively high conversion efficiencies at low input and low output powers. However, for many applications both high conversion efficiency and high output powers are desired. For example, recent work has shown that one can use high performance second harmonic (SH) generation to up-convert the frequency of a squeezed vacuum field [8]. Furthermore, observations of frequency comb

generation in second-order free-space resonator devices [9, 10] has driven further understanding of these systems [11] and are generating demand for high performance, high-power, second-order devices. The integration of devices such as these is the natural step towards moving these technologies into the commercial realm. Unfortunately, the performance of waveguides has traditionally been limited due to a number of factors such as large waveguide losses, poor mode shape profile and high-power effects such as the photorefractive effect. Only recently have large improvements in stable, high conversion efficiency and high-power waveguides been realized. The most common architecture used to this aim is MgO:LiNbO₃ ridge waveguides [6, 12–16]. Sun *et al* have recently produced single-pass waveguides with internal SH conversion efficiencies of around 70% and with output powers exceeding 400 mW at 532 nm [13] and Li *et al* have more recently shown that tailoring the periodic poling can lead to higher output powers (up to 1.13 W at 532 nm) in single-pass [12].

One can further enhance the strength of the nonlinear interaction by resonating the optical field within the waveguide. This method of enhancement has been demonstrated by various groups in a number of different architectures, albeit

¹ Author to whom any correspondence should be addressed.

at low operational powers [17–21]. Resonators also allow one to shape the spectrum of the output light [17] and to tailor the system for optimum conversion for a given pump power and waveguide loss [18]. Despite these benefits, investigation of waveguide resonators for *high-power* and *high conversion efficiency* applications has not been experimentally realized. This is likely due to increased sensitivity to temperature fluctuations (over their single-pass counterparts) as well as traditionally high waveguide losses. Titanium indiffused waveguides exhibit the lowest losses observed from any nonlinear waveguide technology, with losses as low as 0.02 dB cm^{-1} [17]. Ridge waveguides have shown measured losses as low as 0.1 dB cm^{-1} , [22]. At the same time, ridge waveguides have demonstrated single-pass SH conversion efficiencies of around $240\% \text{ W}^{-1} \text{ cm}^{-2}$ (for SH at 340 nm) [14] whilst titanium indiffused waveguides produced in our group have shown single-pass SH conversion efficiencies up to around $40\% \text{ W}^{-1} \text{ cm}^{-2}$ in short samples.

Due to the low losses exhibited in titanium indiffused waveguides, the resonator was produced using this technology. Indiffused waveguides also have a very high spatial overlap with single mode fibers (of up to around 94%, necessary for achieving a high external conversion efficiency). The major disadvantage of titanium indiffused waveguides is the presence of the photorefractive effect [23–26]. Whilst this effect can be compensated for at lower operational powers, the photorefractive effect may enter a chaotic regime at higher powers (also known as chaotic photorefracton) and will produce large amounts of noise on the produced second harmonic generation (SHG) [27].

In this paper, we present the realization of a high-power waveguide resonator, whose external SH conversion efficiency (defined here as the amount of SH power exiting the device divided by the amount of fundamental power incident on the device) is shown to be as high as 75%. The resonance condition has also been locked using a Pound–Drever–Hall (PDH) type locking scheme with feedback to the laser frequency [28], resulting in a reduced conversion efficiency of slightly more than 50%, but with stable output power of up to around 30 mW over an hour.

The device highlights the previously unadvertised performance capabilities and limitations of titanium indiffused waveguides as resonators in applications where high-power and low losses are important. Whilst the wavelength of the converted light from this particular device is easily accessible by various laser technologies, it does provide access to a phase congruent fundamental (which lies in the communications band) and SH field. This is useful, for example, in nonlinear optics experiments that pump any process with the SH of the field such as parametric amplification and oscillation [2], as well as detection of these states using, for example, balanced homodyne detection [29, 30].

2. The waveguide SHG device

Waveguides are fabricated in z-cut LiNbO_3 by an indiffusion of lithographically patterned $7 \mu\text{m}$ wide, 80 nm thick titanium strips at 1060°C for 9 h. In order to mitigate LiO_2 outdiffusion, the diffusion takes place in a platinum box in a diffusion tube that is flushed with oxygen. A second lithography step provides

an insulating photoresist pattern for electric field periodic poling. Finally, in order to reduce stress at the domain walls the sample is annealed at 300°C for 2 h. We have chosen a poling period of approximately $17.0 \mu\text{m}$ to achieve the desired Type 0 quasi-phase matching at a temperature of around 180°C , in order to reduce photorefractive damage [31]. A short sample length of 8 mm long is chosen as a smaller sample is easier to stabilize in temperature and ensures that phase matching is uniform across the entire sample. For all measurements, the sample is heated to the ideal phase matching temperature of around 180°C .

In order to optimize the conversion efficiency, one needs to correctly choose the mirror coating reflectivities. We choose to have the SH exit the rear of the sample whilst the pump enters through the front, as illustrated in figure 1. The rear surface therefore has an anti-reflection (AR) coating at 775 nm and a high-reflectivity (HR) coating for 1550 nm. The front surface is coated with a 77% mirror at 1550 nm and a HR coating at 775 nm, thereby resulting in a double-pass configuration for the SH field [32]. The 77% coating is chosen to achieve optimal coupling of the pump assuming linear intra-cavity losses of 0.07 dB cm^{-1} and a pump power of approximately 50 mW using the expected nonlinear properties of the device [18]. Note that finding this working point is not as trivial as finding the standard critical coupling in the non pump-depleted regime because the large nonlinear ‘loss’ on the fundamental field due to upconversion has to be taken into account (One can find the optimum working point using the theory described in section 3.2.2). The coatings for the device are produced in-house using ion-beam assisted vapor deposition. Lithium niobate ‘witness samples’ are coated in the same coating runs and from these the properties of the coatings are determined (using an Agilent Cary5000 spectrophotometer, which has a specified transmittance error of approximately 0.2% at 1550 nm). The HR coatings are expected to have a reflectivity greater than 99%, and AR coatings a reflectivity of around 0.5%. We note that the performance of the double-pass SH device depends critically on the phase relationship between the forward and reverse-propagating fields. To address this issue, the waveguide sample consists of many (around 100) waveguides. The polishing of the waveguide sample end-faces is not perfectly parallel and therefore the phase relationship varies from waveguide to waveguide and provides a means for searching over this parameter [32].

3. Waveguide resonator characterization

3.1. Linear properties

We begin by determining the linear properties of the device at the fundamental wavelength of 1550 nm. Using the standard Fabry–Perot equations, one can find expressions for the ratios between the transmitted power and the power entering the waveguide mode ($P_{\text{trans}}/P_{\text{in}}$) as well as the reflected power and the incident power on resonance ($P_{\text{ref}}^{\text{on}}/P_{\text{in}}$) [33],

$$\frac{P_{\text{ref}}^{\text{on}}}{P_{\text{in}}} = \frac{(\sqrt{R_f} - \sqrt{R_r} e^{-\alpha L})^2}{(1 - \sqrt{R_f R_r} e^{-\alpha L})^2}, \quad (1)$$

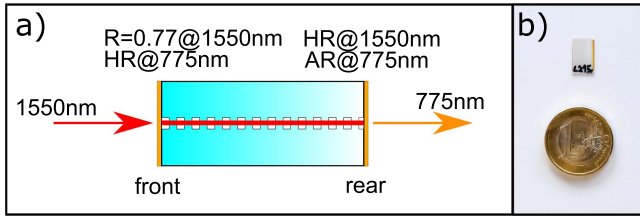


Figure 1. A schematic of the device is shown in (a). A pump field at 1550 nm is incident on the front coating of the device and the generated second harmonic escapes the sample from the coating on the rear. Only a single waveguide and a representation of its periodic poling is shown and is not to scale. A photograph of a similar waveguide sample is shown in (b).

$$\frac{P_{\text{trans}}}{P_{\text{in}}} = \frac{(1 - R_f)(1 - R_r)e^{-\alpha L}}{(1 - \sqrt{R_f R_r} e^{-\alpha L})^2}, \quad (2)$$

where L is the sample length in centimeters, α is the loss rate per centimeter of the fundamental field, R_f is the power reflectivity for the front mirror and R_r is the power reflectivity for the rear mirror. If the reflectivity of the front mirror is well known, then these equations can be solved to find the intra-cavity loss rate and the reflectivity of the HR mirror.

The experimental layout is shown in figure 2. The waveguide is pumped by a Tunicas tunable C-band laser that is amplified using an EDFA. For this measurement the wavelength of the laser is offset by 10 nm, such that the phase matching condition is *not* met, thereby removing the nonlinear interaction. The light passes through a Faraday isolator that is used to measure the light reflected by the cavity, at PD1. The light then passes through an EOM, later used in combination with the Toptica digilock system (which consists of a high voltage amplifier, a mixer and a waveform generator) for locking the cavity length. The feedback signal from this locking system can be connected to the waveguide heater or the laser frequency control. The power can then be fine-tuned using a half-wave plate followed by a polarizing beam-splitter. A dichroic mirror before the front surface of the waveguide can be used to measure the amount of SH light leaking from the coating on this surface incident at PD2. A second dichroic mirror at the exit of the waveguide separates the transmitted pump light, which can be measured at PD4, from the generated SH light, which is measured at PD3. All of the relevant light powers are then measured using a Thorlabs PM100 power meter and are cross-referenced using the photodetectors in the setup, ensuring that all results are consistent.

For accurate conversion efficiency measurements the mode overlap between the (fiber-coupled) laser mode and the waveguide mode is first precisely determined. The coupling of the laser beam into the mode of the waveguide is optimized and the light transmitted through the cavity is then coupled into a fiber as shown in figure 2. The fiber containing the laser field is then disconnected from the experiment and reconnected to this rear fiber-coupling, resulting in the laser field entering the waveguide from the rear surface. The Faraday isolator is then removed such that the light transmitted through the front face of the cavity (and therefore in the cavity

spatial mode) is incident upon the fiber coupler. One can then measure the amount of power incident on and exiting the first fiber coupler to determine a lower bound for the mode overlap. From this measurement, the overlap between the fiber mode and the waveguide mode is determined to be 0.93 ± 0.02 .

Next, approximately $300 \mu\text{W}$ of power is coupled into the waveguide cavity. The laser frequency is scanned and on reflection we find that the power on resonance is $36\% \pm 1\%$ of the power off resonance. We also find that the transmitted power on resonance is $6.3\% \pm 0.1\%$ of the power entering the cavity. Inserting these values into the ratios derived from equations (1) and (2), one finds that the intra-cavity loss at the fundamental wavelength is $\alpha = 0.16 \pm 0.01 \text{ dB cm}^{-1}$ and the reflectivity of the rear mirror at the fundamental wavelength is $99.4\% \pm 0.1\%$. The waveguide loss for the SH field is typically found to be a factor of 2 or 3 greater than that found for the fundamental field and here we assume that $\alpha_{2\omega} = 2\alpha$. Using these values one can now determine the cavity finesse $F = \frac{\pi\sqrt{r}}{1-r} = 20$, free spectral range $\text{FSR} = \frac{c}{2Ln} = 8.7 \text{ GHz}$ and cavity linewidth $\nu = \frac{\text{FSR}}{F} = 440 \text{ MHz}$; where n is the refractive index of the fundamental wave and $r = \sqrt{R_f R_r R_t}$. The loss is unfortunately higher than desired, this is due to the fact that it is necessary to find a waveguide with the right phase matching condition, a high nonlinear conversion efficiency and low losses. This waveguide is the best compromise of the three parameters on this particular device.

3.2. Conversion efficiency

3.2.1. Non pump-depleted regime. With the fundamental cavity well characterized, attention is now turned to the nonlinear properties of the device. We begin our treatment in the low-power regime, where analytic solutions can be found and from these the desired parameters can be determined. To further simplify the treatment, it is assumed that the coating on the front face does not transmit any power at 775 nm and that the coating on the rear face perfectly transmits power at this wavelength. The normalized (single-pass) internal conversion efficiency, η_{norm} , is first defined,

$$\eta_{\text{norm}} = \frac{P_{\text{SH}}}{P_{\text{in}}^2 L^2}, \quad (3)$$

where P_{SH} is the SH power exiting the waveguide resonator at the rear surface and P_{in} is the pump power entering the waveguide mode.

The resonator provides an intra-cavity build-up of the pump field, which can be characterized with the build-up factor, f [18],

$$f = \frac{1 - R_f}{(1 - \sqrt{R_f R_r} e^{-\alpha L})^2}. \quad (4)$$

This build-up factor can be combined with the single-pass normalized conversion efficiency to determine the conversion efficiency of the resonant device. The conversion efficiency

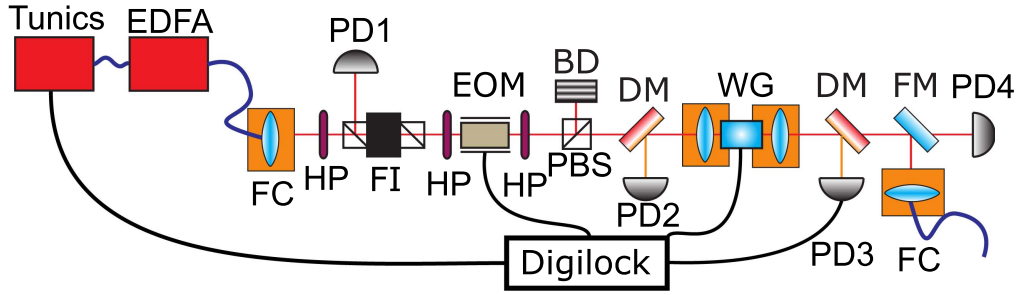


Figure 2. Experimental layout. Tunics: tunics 1550 nm tunable laser, EDFA: erbium-doped fiber amplifier, FC: fiber coupler, PD: photodetector, FI: Faraday isolator, HP: half-wave plate, EOM: electro-optic phase modulator, PBS: polarizing beam-splitter, BD: beam dump, WG: temperature-controlled waveguide, DM: dichroic mirror, FM: flipper mirror.

(in the absence of pump depletion) for the double-pass pump-resonant device described here is defined [18, 32],

$$\frac{P_{SH}}{P_{in}} \approx 2\eta_{norm} h P_{in} f^2 (2 - 2\cos(\theta)), \quad (5)$$

where θ represents the relative phase shift between the SH and fundamental fields due to the HR mirror at 775 nm on the front surface of the device and the width of the domain adjacent to this coating. The term in the parentheses represents the interference between the forward- and reverse-generated fields. It can be seen that constructive interference between these two waves, given by $\theta = (2m - 1)\pi$ where $m \in \mathbb{Z}$, results in a factor of 4 improvement in the conversion efficiency. The conversion efficiency of the double-pass device with an ideal phase shift is therefore identical to a device operated at the same power with a length of $2L$. The waveguide length is replaced by the loss-corrected form, h , and is given by [18],

$$h = \left(\frac{e^{-\alpha L} - e^{-\alpha_{2\omega} L/2}}{\alpha - \alpha_{2\omega}/2} \right)^2, \quad (6)$$

where $\alpha_{2\omega}$ is the waveguide loss for the SH wave. Note that h reduces to L^2 in the limit that the losses go to zero and that L'Hôpital's rule must be used when $\alpha_{2\omega} = \alpha$.

The conversion efficiency of the device is determined by measuring the SH power exiting the rear surface of the device as the pump power is varied. The pump power entering the waveguide is varied through rotation of a half-wave plate in the beam path and through varying the fiber amplifier gain. The frequency of the laser is scanned (using a triangle function with an amplitude that corresponds to a laser frequency shift of 3 GHz at a scanning rate of approximately 20 Hz) such that the laser frequency passes through one resonance of the cavity. Note that the zero frequency reference is chosen arbitrarily. The central wavelength of the laser is then shifted such that the optimal cavity resonance, the one that is closest to the center of the phase matching curve, is found. Due to the fact that thermal heating is dependent on the amount of SH power and fundamental power, which both depend on the phase matching and resonance conditions, further fine tuning is then required to fully optimize the SH production. The generated SH power on resonance is detected on PD3 after attenuation via a calibrated

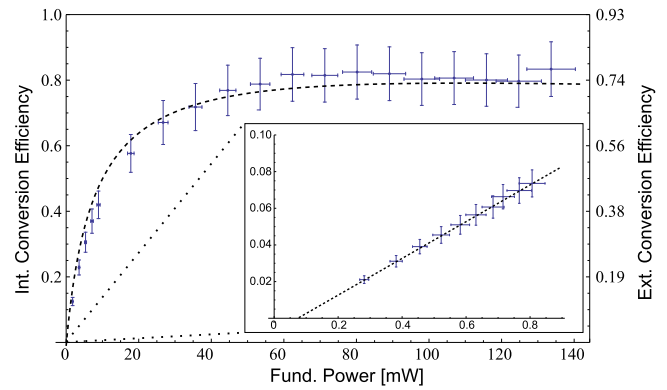


Figure 3. Measured conversion efficiency of the waveguide resonator in both the high-power and low-power regimes. The main figure shows the high-power measurements (blue dots) and the solution to the coupled equations (dashed line), equations (7) and (8). The inset shows a zoom-in on the low-power regime, showing a fit of equation (5) (dashed line) to the low-power data (blue dots). The offset from the origin is due to the offset from the photodetectors. Data points are shown with error bars.

neutral density filter. These results are cross-checked for consistency using power meter measurements.

Figure 3 shows the measured conversion efficiency of the device as the input pump power is varied and the generated SH power is measured. A high-power run is shown in the main figure, while the inset shows a zoom-in on the low-power regime. The inset shows a fit to the data using the model described in equation (5). The only free parameter for the fit is the nonlinear coupling coefficient, which is found to be $\kappa = 0.71$. The internal conversion efficiency is defined as the SH power exiting the waveguide divided by the pump power matching the waveguide mode. Note that the relative phase shift θ and exact magnitude of the normalized conversion efficiency both affect the conversion efficiency of the device and cannot be independently determined. However, if one assumes that the phase shift gives complete constructive interference $\theta = (2m - 1)\pi$ where $m \in \mathbb{Z}$, then the best fit of the conversion efficiency (using equation (5)) requires a normalized nonlinear conversion efficiency of $38\%/(\text{W cm}^2)$. This value coincides with the expected value from both theory [18] and previous measurements of other samples with similar length, thereby giving us confidence in the initial assumption about the phase. Using mode size

measurements from similar waveguides and RSoft simulations, which give us an expected effective interaction area [18] of $85 \mu\text{m}^2$, we determine the nonlinear coefficient to be $d_{\text{eff}} = 26 \text{ pm V}^{-1}$. The d_{eff} is not precisely known at 1550 nm but it has been measured to be 20 pm V^{-1} at 1330 nm and up to 34 pm V^{-1} at shorter wavelengths [34].

3.2.2. Pump depletion regime. The expected performance of the device at higher powers (the main part of figure 3), where the non pump-depleted approximation is no longer valid, is found by numerically solving the coupled-mode equations in the same way as presented by Fujimura *et al* [35]. The coupled-mode equations for perfect phase matching are written,

$$\frac{d}{dz}A(z) = -i\kappa^*B(z)A(z)^* - \frac{\alpha}{2}A(z), \quad (7)$$

$$\frac{d}{dz}B(z) = -i\kappa[A(z)]^2 - \frac{\alpha_{2\omega}}{2}B(z), \quad (8)$$

where $A(z)$ and $B(z)$ are the complex amplitudes for the fundamental and SH waves, respectively, and κ is the nonlinear coupling coefficient. We assume here that κ is real because the low-power modeling has shown that our system is well modeled under the assumption of perfect constructive interference between the forward and reverse traveling waves, or in other words, no phase shift on the quasi-phase matching grating.

A brief summary of the iterative method is described here, a full description can be found in [35]. At each end-face the internal fields are separated into forward and reverse traveling components. By assuming some initial conditions the coupled equations can be solved. These solutions are then checked for self-consistency with the initial conditions to ensure a meaningful result. If the fields are not self-consistent then a new initial condition is calculated based on the result of the previous iteration until self-consistency is reached. After many iterations a self-consistent solution for the internal fields is found, from which the external fields can be calculated using the boundary conditions. Given the external fields, the internal conversion efficiency of the device is calculated, as shown in the main part of figure 3 (dashed line). The nonlinear coupling coefficient $\kappa = 0.71$ from the fit of equation (5) in the low-power regime is used and all other parameters are as used in the low-power regime fit. Note that the high-power theory curve therefore has no free parameters, and still reasonably predicts the behavior of the system. Furthermore, closer examination reveals that the non pump-depleted theory and the full theory taking pump depletion into account are effectively indistinguishable over the power range illustrated in the inset of figure 3, as one would expect.

The external conversion efficiency is defined as the SH power exiting the waveguide divided by the input pump power directly before the waveguide in-coupling lens. Note that the pump power measured in this way includes losses due to imperfect overlap between the pump and waveguide modes. It can be seen that an external conversion efficiency of 75% is achieved for input powers of around 70 mW, which we stress is achieved when the frequency of the laser is scanned over the cavity resonance. In section 5, it will be

shown that we are unable to stabilize the cavity length at this power, nevertheless this scanning mode of operation may be useful for some applications. At fundamental input powers of 140 mW and above the maximum transmitted power level seen as the laser was scanned over resonance was observed to rapidly fluctuate. This behavior may indicate that the photorefractive effect has entered the chaotic regime, but may also be due to other instabilities arising due to the high-power levels, such as third-order nonlinearities or photo-thermal instabilities. This is investigated further in the following section.

4. High-power limitations

The high-power performance of the device is limited by photothermal and/or photorefractive effects. These effects are difficult to distinguish due to the fact that they are both expected to shift the cavity resonance in a similar fashion [36]. It is expected that as the device produces more power the magnitude of these effects will increase and the task of keeping the resonator on resonance will become more difficult.

Whilst it is difficult to get a quantitative analysis of these effects, it is possible to look at them qualitatively. By scanning the frequency of the laser one can scan over the cavity resonance approaching from both high and low frequency sides while detecting the transmitted power on PD4 (see figure 2). The presence of photothermal heating will produce an asymmetric pump transmission around the resonance frequency in response to the laser frequency scan. This is because as resonance is approached from one side, heating of the cavity will tend to bring the cavity closer to resonance, leading to a very rapid transition to resonance. Approaching resonance from the opposite side will then cause heating that pushes the system away from resonance. A similar explanation can be formulated for the photorefractive effect. In fact, both effects are expected to affect the refractive index in a similar way, and hence the two can be difficult to distinguish [37].

Such a cavity scan is shown in figure 4, where approximately 110 mW of fundamental light is incident on the cavity. The direction of the laser frequency scan (scanned using a triangle function) is reversed at around zero seconds. The black trace shows the transmitted fundamental power when the cavity temperature is held at phase matching, resulting in a SH power of around 70 mW. We note that the expected Airy function describing the transmitted power through the cavity is not seen. Instead an asymmetric function of transmitted power is found, indicating some minor amount of photothermal and/or photorefractive effects.

To investigate the wavelength dependence of the asymmetry the frequency of the laser was varied, such that the device was far from phase matching and no SH power was produced. The transmitted power was again measured as the cavity was scanned and is shown by the blue trace. One immediately notices that, as expected, the cavity bandwidth has reduced due to both the absence of the nonlinear ‘losses’ on the fundamental field (which reduce the finesse of the

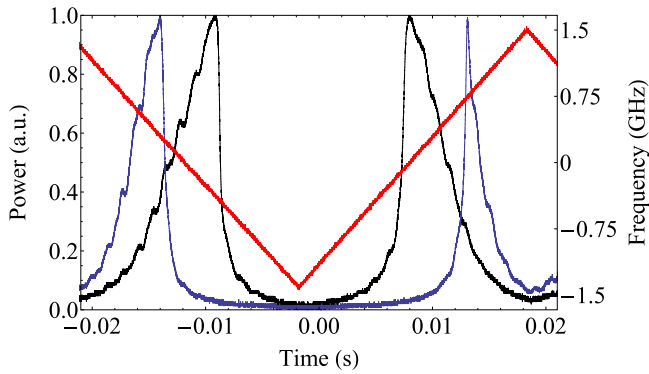


Figure 4. Measured transmitted fundamental power (left axis) with the cavity temperature on- (black trace) and off- (blue trace) phase matching. Approximately 110 mW of fundamental power enters the sample as the frequency of the laser is scanned over resonance with a triangle function (red trace), the magnitude of which corresponds to a laser frequency shift of 3 GHz (right axis). The oscillations on top of the cavity scan are due to interferences caused by the laser frequency scan.

fundamental cavity) and the absence of the SH field, which is expected to have a higher absorption and hence provide more heating. However, a large asymmetry is still seen, the magnitude of which is similar to that seen in the phasematched case. The strength of the photorefractive effect is expected to increase by orders of magnitude between the pump and SH wavelengths [36], whilst the absorption is typically seen to only increase by a factor of 2 or 3 between these wavelengths. We also note that the profile of the transmitted power in the off-phase matching case is dependent upon which direction the cavity resonance is approached from. This is the expected behavior in the presence of photothermal heating of the cavity system due to the fact that the cavity resonance will always shift towards one direction [38] and is more apparent in this case due to the increased cavity finesse when the system is far from phase matching.

The observed results therefore indicate that there is not a significant contribution from photorefractive effects. Raising the temperature of the system has most likely reduced the photorefractive effect to a point where the performance of the device under these conditions is not limited by the effect. We therefore conclude that the observed instabilities in the device are most likely not due to photorefractive effects.

5. Stability

The stability of frequency conversion devices is a critical factor in many applications. One typically requires device stability that is at least equal to the required measurement time. Therefore, a preliminary investigation into device stability over longer time periods is undertaken. Note that there is very little prior information regarding the long-term stability of high-power waveguide resonators. Due to the narrow linewidth of the cavity resonance this requires very stable,

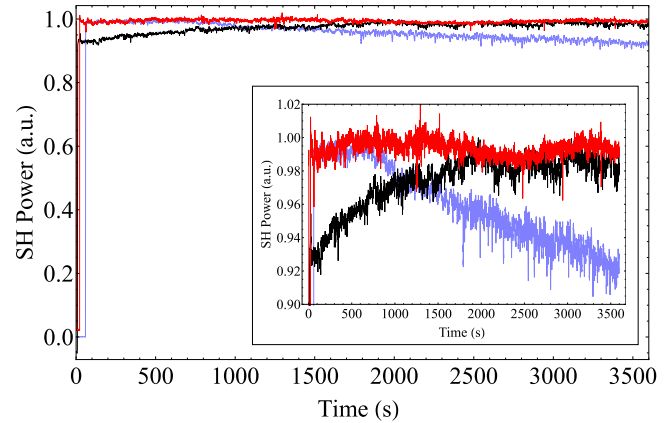


Figure 5. Output power of the SHG device over one hour with a temperature (blue) feedback loop and a low-power (red) and high-power (black) laser feedback loop enabled. The output SH power is normalized to the amount of power seen after the system has stabilized over a few minutes. The inset shows a zoomed in view of the data.

fine temperature tuning and for greater stability, some form of feedback that locks to the cavity resonance.

The issue of stability is addressed in two steps. The first step is to optimize the standard temperature loop that heats the sample to around 180 °C. The two-stage oven is enclosed in a Teflon housing and is then encased in a larger housing with openings only for the input and output fields. With this setup the temperature of the cavity is stable to a couple of millikelvin or better and this is enough to ensure that the cavity resonance is held, at low input powers and without the PDH loop, on the minute time scale. This scheme is limited because it does not sense the resonance condition. As such, system drifts may force the cavity off resonance in a way that is not sensed by the temperature sensor in this loop and are therefore not compensated. A second step is required to provide stability over longer time scales and at higher powers.

The second step is the PDH locking loop which directly senses the resonance condition (of the fundamental field), thereby providing a means of compensating system drift over longer times. This locking loop was first achieved for low powers. The field entering the waveguide resonator is phase modulated via an electro-optic modulator at 25 MHz, as shown in figure 2. Its sidebands are well within the cavity linewidth and as such are transmitted through the cavity with the carrier and are detected at PD3. This signal is then fed into a Toptica Digilock system, therein undergoing mixing and filtering to produce the error signal. This error signal is then used to lock the system to resonance via feedback. It is possible to achieve this feedback via two methods; the first is by feeding back to the temperature controller of the waveguide, and the second by feeding back to the laser frequency through actuation of a piezoelectric transducer. Feeding back to the laser provides a much faster lock but results in the center frequency of the laser shifting, which will be an unwanted effect for some applications.

The performance of the two low-power locking schemes is illustrated in figure 5. The temperature feedback lock (blue

Table 1. Comparison of selected waveguide SH performances. λ_{SH} is the second harmonic wavelength (nm), P_{SH} is the maximum second harmonic power generated (mW), Ext. is the external conversion efficiency (where N.G. = not given), Int. is the external conversion efficiency (where N.G. = not given), material is the waveguide material used (Ti:LN = titanium indiffused lithium niobate, MgO:LN = magnesium oxide doped lithium niobate), Sch. is the scheme used (where Res. = resonator and S.P. = single-pass), and stab. is whether or not the device stability has been shown over at least one hour (Y = yes and N = no). ¹ Note that this paper does not specify how the pump power is measured, here we have assumed the maximum possible value.

Paper	λ_{SH}	P_{SH}	Ext.	Int.	Material	Sch.	Stab.
This paper	775	110	75%	84%	Ti:LN	Res.	Y
Li 2017 [12]	532	1130	$\approx 75\%$ ¹	N.G.	MgO:LN	S.P.	N
Sun 2012 [13]	532	466	$\approx 40\%$	70%	MgO:LN	S.P.	N
Jechow 2007 [39]	488	100	24%	38%	MgO:LN	S.P.	Y
Sakai 2006 [15]	488	73	N.G.	27%	MgO:LN	S.P.	Y
Iwai 2003 [6]	473	189	$\approx 30\%$	74%	MgO:LN	S.P.	Y
Mizuuchi 2003 [14]	340	22	N.G.	28%	MgO:LN	S.P.	N
Parameswaran 2002 [40]	775	420	47%	N.G.	MgO:LN	S.P.	N
Regener 1988 [18]	546	0.002	0.1%	N.G.	Ti:LN	Res.	N

trace) is performed with approximately 30 mW of fundamental field entering the cavity, resulting in approximately 10 mW of SH power generation, whilst the laser feedback scheme (red trace) has approximately 22 mW of fundamental field entering the cavity and 9 mW SH power exiting the system. As expected, the temperature feedback scheme does not perform as well as the laser frequency feedback as an accumulated offset is observed, likely due to the cavity resonance condition shifting away from the peak of the phase matching as the localized temperature of the waveguide shifts due to heating of the sample. In contrast, at the powers used here the laser feedback scheme locks to the maximum power immediately and has been locked stably for more than 6 h, the first hour of which is illustrated in figure 5.

In order to achieve a more stable lock at higher pump powers, the quality of the lock has to be improved. The Tunics laser is replaced with a New Focus velocity laser, providing a greater tuning range for the laser feedback. Furthermore, an integrated phase modulator allows for higher frequency modulation (of 302 MHz), improving the capture range and allowing for detection of these sidebands on reflection of the cavity where the beat signal is stronger (with a fiber integrated photodiode replacing PD2). Approximately 52 mW of fundamental field enters the cavity and the SH power stabilizes to around 28 mW of SH after approximately 20 minutes, as illustrated by the black trace of figure 5. This level of combined performance; high conversion efficiency, high-power, and long-term stability, has not been presented previously from a waveguide resonator and highlights the versatility and quality of this device.

Currently, it is not possible to stably lock the SH cavity at higher input pump power. In contrast to the seemingly random fluctuations seen when scanning resonance with a pump power of 140 mW, pumping the locked cavity above 50 mW results in the output SH power oscillating between two distinct output power levels, the frequency of which is dependent on the exact amount of pump power, but is typically on the time scale of seconds. Imaging the output SH spatial mode onto a camera reveals that the output SH mode hops between two possible spatial modes. This effect requires a drastic

change in the phase matching properties of the system and therefore may be due to a localized photorefractive effect or even a Kerr effect. Operation at higher powers will require an understanding of this effect if one wishes to operate the system with a stable continuous-wave output.

6. Discussion

For ease of comparison, the main results from this work are compared to previous waveguide SHG results in table 1. It can be seen that waveguide resonators as a source of high performance SH generation have been overlooked since the results of Regener *et al* in 1988. However, the results presented in this paper clearly show that waveguide resonators can indeed be used in demanding applications, *even in the pump-depleted regime*, as we demonstrate here for the first time. In addition, we have shown for the first time that titanium indiffused waveguide SHG devices are capable of producing tens of milliwatts of SH power stabilized over long time scales, a critical performance measure for both research and commercial applications. These results will be of interest in a number of fields where high performance devices are required, for example, in integrated quantum optics where the external conversion efficiency is often paramount [8].

7. Conclusion

In conclusion, we demonstrated a high external conversion efficiency, high-power, SH waveguide resonator device. This was achieved in an 8 mm long titanium indiffused lithium niobate waveguide device. With a 1550 nm pump field, an external conversion efficiency of 75% was measured as the laser frequency was scanned, with output powers up to 110 mW. The device was locked stably over an hour using a PDH scheme producing 28 mW of SH power (conversion efficiency greater than 50%) via a laser frequency feedback scheme. The results presented here showcase the suitability of

titanium indiffused waveguide resonators for high-power, low loss applications.

Acknowledgments

The authors acknowledge funding from DFG (Deutsche Forschungsgemeinschaft) via the Gottfried Wilhelm Leibniz-Preis.

ORCID iDs

M Stefszky  <https://orcid.org/0000-0001-5379-3460>

C Silberhorn  <https://orcid.org/0000-0002-2349-5443>

References

- [1] Woote E L *et al* 2000 A review of lithium niobate modulators for fiber-optic communications systems *IEEE J. Sel. Top. Quantum Electron.* **6** 69
- [2] Arbore M A and Fejer M M 1997 Singly resonant optical parametric oscillation in periodically poled lithium niobate waveguides *Opt. Lett.* **22** 151
- [3] Anderson M E, Beck M, Raymer M G and Bierlein J D 1995 Quadrature squeezing with ultrashort pulses in nonlinear-optical waveguides *Opt. Lett.* **20** 620
- [4] Stefszky M, Ricken R, Eigner C, Quiring V, Herrmann H and Silberhorn C 2017 Waveguide cavity resonator as a source of optical squeezing *Phys. Rev. Appl.* **7** 044026
- [5] Rütz H, Luo K-H, Suche H and Silberhorn C 2016 Towards a quantum interface between telecommunication and UV wavelengths: design and classical performance *Appl. Phys. B* **122** 13
- [6] Iwai M, Yoshino T, Yamaguchi S, Imaeda M, Pavel N, Shoji I and Taira T 2003 High-power blue generation from a periodically poled MgO:LiNbO₃ ridge-type waveguide by frequency doubling of a diode end-pumped Nd:Y₃Al₅O₁₂ laser *Appl. Phys. Lett.* **83** 3659
- [7] Vandevender A P and Kwiat P 2004 High efficiency single photon detection via frequency up-conversion *J. Mod. Opt.* **51** 1433
- [8] Vollmer C E, Braune C, Sambrowski A, Eberle T, Händchen V, Fiuřášek J and Schnabel R 2014 Quantum up-conversion of squeezed vacuum states from 1550 to 532 nm *Phys. Rev. Lett.* **112** 073602
- [9] Ulvila V, Phillips C R, Halonen L and Vainio M 2013 Frequency comb generation by a continuous-wave-pumped optical parametric oscillator based on cascading quadratic nonlinearities *Opt. Lett.* **38** 4281
- [10] Ricciardi I, Mosca S, Parisi M, Maddaloni P, Santamaria L, De Natale P and De Rosa M 2015 Frequency comb generation in quadratic nonlinear media *Phys. Rev. A* **91** 063839
- [11] Leo F, Hansson T, Ricciardi I, De Rosa M, Coen S, Wabnitz S and Erkintalo M 2016 Walk-off-induced modulational instability, temporal pattern formation, and frequency comb generation in cavity-enhanced second-harmonic generation *Phys. Rev. Lett.* **116** 033901
- [12] Li G and Cui Y 2017 High power continuous wave second harmonic generation in a phase matching insensitive mgo doped linbo3 waveguide *Opt. Express* **25** 29225–32
- [13] Sun J and Xu C 2012 466 mW green light generation using annealed proton-exchanged periodically poled MgO:LiNbO₃ ridge waveguides *Opt. Lett.* **37** 2028
- [14] Mizuuchi K, Sugita T, Yamamoto K, Kawaguchi T, Yoshino T and Imaeda M 2003 Efficient 340 nm light generation by a ridge-type waveguide in a first-order periodically poled MgO:LiNbO₃ *Opt. Lett.* **28** 1344
- [15] Sakai K, Koyata Y and Hirano Y 2007 Blue light generation in a ridge waveguide MgO:LiNbO₃ crystal pumped by a fiber Bragg grating stabilized laser diode *Opt. Lett.* **32** 2342
- [16] Sakai K, Koyata Y and Hirano Y 2006 Planar-waveguide quasi-phase-matched second-harmonic-generation device in Y-cut MgO-doped LiNbO₃ *Opt. Lett.* **31** 3134
- [17] Luo K-H, Herrmann H, Krapick S, Brecht B, Ricken R, Quiring V, Suche H, Sohler W and Silberhorn C 2015 Direct generation of single-longitudinal-mode narrowband photon pairs *New J. Phys.* **17** 073039
- [18] Regener R and Sohler W 1988 Efficient second-harmonic generation in Ti:LiNbO₃ waveguide resonators *J. Opt. Soc. Am. B* **5** 267
- [19] Pernice W H P, Xiong C, Schuck C and Tang H X 2012 Second harmonic generation in phase matched aluminum nitride waveguides and micro-ring resonators *Appl. Phys. Lett.* **100** 223501
- [20] Scaccabarozzi L, Fejer M M, Huo Y, Fan S, Yu X and Harris S 2006 Enhanced second-harmonic generation in AlGaAs/Al₂O₃ tightly confining waveguides and resonant cavities *Opt. Lett.* **31** 3626–8
- [21] Fujimura M, Sudoh M, Kintaka K, Sahara T and Nishihara H 1996 Resonant waveguide quasi-phase-matched SHG devices with electrooptic phase-modulator for tuning *IEEE J. Sel. Top. Quantum Electron.* **2** 396
- [22] Gui L, Hu H, Garcia-Granda M and Sohler W 2009 Local periodic poling of ridges and ridge waveguides on X- and Y-Cut LiNbO₃ and its application for second harmonic generation *Opt. Express* **17** 3923–8
- [23] Nava S G, Minzioni P, Cristiani I, Argiolas N, Bazzan M, Ciampolillo M V, Pozza G, Sada C and Degiorgio V 2013 Photorefractive effect at 775 nm in doped lithium niobate crystals *Appl. Phys. Lett.* **103** 031904
- [24] Pal S, Das B K and Sohler W 2015 Photorefractive damage resistance in Ti:PPLN waveguides with ridge geometry *Appl. Phys. B* **120** 737
- [25] Becker R A and Williamson R C 1985 Photorefractive effects in LiNbO₃ channel waveguides: model and experimental verification *Appl. Phys. Lett.* **10** 1024
- [26] Kondo Y, Miyaguchi S, Onoe A and Fujii Y 1994 Quantitatively measured photorefractive sensitivity of proton-exchanged lithium niobate, proton-exchanged magnesium oxide-doped lithium niobate, and ion-exchanged potassium titanyl phosphate waveguides *Appl. Opt.* **33** 3348
- [27] Carrascosa M, Villaeroel J, Carnicero J, Garcia-Cabañes A and Cabrera J M 2008 Understanding light intensity thresholds for catastrophic optical damage in LiNbO₃ *Opt. Express* **16** 115
- [28] Black E D 2001 An introduction to Pound–Drever–Hall laser frequency stabilization *Am. J. Phys.* **69** 79
- [29] Stefszky M S, Mow-Lowry C M, Chua S S Y, Shaddock D A, Buchler B C, Vahlbruch H, Khalaidovski A, Schnabel R, Lam P K and McClelland D E 2012 Balanced homodyne detection of optical quantum states at audio-band frequencies and below *Class. Quantum Grav.* **29** 145015
- [30] Mehmet M, Ast S, Eberle T, Steinlechner S, Vahlbruch H and Schnabel R 2011 Squeezed light at 1550 nm with a quantum noise reduction of 12.3 dB *Opt. Express* **19** 25763
- [31] Carrascosa M and Arizmendi L 1993 High-temperature photorefractive effects in LiNbO₃:Fe *J. Appl. Phys.* **73** 2709

- [32] Imeshev G, Proctor M and Fejer M M 1998 Phase correction in double-pass quasi-phase-matched second-harmonic generation with a wedged crystal *Opt. Lett.* **23** 165
- [33] Siegman A E 1986 *Lasers* (Mill Valley, CA: University Science Books)
- [34] Shoji I, Kondo T, Kitamoto A, Shirane M and Ito R 1997 Absolute scale of second-order nonlinear-optical coefficients *J. Opt. Soc. Am. B* **14** 2268
- [35] Fujimura M, Suhara T and Nishihara H 1996 Theoretical analysis of resonant waveguide optical second harmonic generation devices *J. Lightwave Technol.* **14** 1899
- [36] Fujiwara T, Sato S and Mori H 1989 Wavelength dependence of photorefractive effect in Ti-indiffused LiNbO₃ waveguides *Appl. Phys. Lett.* **54** 975
- [37] Li G, Cui Y and Wang J 2013 Photorefractive inhibition of second harmonic generation in periodically poled MgO doped LiNbO₃ waveguide *Opt. Express* **21** 21790–9
- [38] Carmon T, Yang L and Vahala K J 2004 Dynamical thermal behavior and thermal self-stability of microcavities *Opt. Express* **12** 4742
- [39] Jechow A, Skoczowsky D and Menzel R 2007 100 mw high efficient single pass SHG at 488 nm of a single broad area laser diode with external cavity using a PPLN waveguide crystal *Opt. Express* **15** 6979–81
- [40] Parameswaran K, Kurz J R, Roussev R V and Fejer M M 2002 Observation of 99% pump depletion in single-pass second-harmonic generation in a periodically poled waveguide *Opt. Lett.* **27** 43